Nonequilibrium multiscale computational model

Xiaohu Liu and Shaofan Li[a)]
Department of Civil and Environmental Engineering, University of California, Berkeley, California 94720

(Received 6 November 2006; accepted 1 February 2007)

A computational multiscale method is proposed to simulate coupled, nonequilibrium thermomechanical processes. This multiscale framework couples together thermomechanical equations at the coarse scale with nonequilibrium molecular dynamics at the fine scale. The novel concept of distributed coarse scale thermostats enables subsets of fine scale atoms to be attached to different coarse scale nodes which act as thermostats. The fine scale dynamics is driven by the coarse scale mean field. A coarse-grained Helmholtz free energy is used to derive macroscopic quantities. This new framework can reproduce the correct thermodynamics at the fine scale while providing an accurate coarse-grained result at the coarse scale. © *2007 American Institute of Physics*. [DOI: 10.1063/1.2711432]

I. INTRODUCTION

The development of nanotechnology poses new challenges for computational physics. Very often we need to simulate problems that traverse different spacial and temporal scales. This gives rise to a class of multiscale simulation methods,[1,2,57] which has become an active research topic in computational science. Until now, most multiscale methods focus on solving problems at zero temperature due to the difficulties to include the temperature effect. Recently, there has been considerable effort devoted on developing finite-temperature multiscale algorithms.[3–7] However, most of the approaches in the literature can only simulate equilibrium systems with a uniform environment temperature.

In this paper, we propose a new multiscale framework that is capable of dealing with more complicated problems, i.e., the steady-state nonequilibrium systems. The method is based on a novel concept of distributed coarse scale thermostats. Under this concept, each coarse scale node is viewed as a thermostat and governs a set of atoms associated with it. Coupled thermomechanical equations are solved at the coarse scale so that each node has its own temperature. Molecular dynamics (MD) is carried out at the fine scale level with distributed thermostats.

Developed in the late 1970s, the nonequilibrium molecular dynamics (NEMD) has long been a successful simulation tool[8–10] for many scientific and engineering problems. NEMD has been widely used to compute transport coefficients[11–13] and simulate viscous flows.[14–16] NEMD extends the equilibrium MD by introducing an external field. For example, the DOLLS algorithm[17,18] and the SLLOD algorithm,[9] both proposed to solve the Couette flow problem, include prescribed shear strain rate, a macroscopic quantity in molecular dynamics equations of motion (EOMs) to deduce the desired dynamics. However, in current NEMD methods the external fields are usually constant, which poses difficulties when applying to general Navier-Stokes equations and thermomechanical problems. In this paper, the proposed multiscale method extends the NEMD approach by introducing the coarse scale velocities and accelerations as external fields. They drive the fine scale atomistic system off the equilibrium state. Furthermore, subsets of the atoms in the fine scale model are associated with different coarse scale nodes, acting as thermostats. Via multiscale coupling, the fine scale model can provide atom-level details for nonequilibrium phenomenon that conventional NEMD cannot simulate.

In multiscale computation, it is very important to have a coarse scale model that is consistent with the fine scale atomistic model. This requires the coarse scale quantities such as the stress to be derived from the knowledge of atomistic interactions instead of an empirical potential. The most popular approach to realize this is by coarse graining. Among several methods of this category,[18,19] the quasicontinuum (QC) method[20,21] is the most notable. In the QC method, a coarse-grained internal energy is obtained based on the Cauchy-Born rule. One limitation of the original QC approach is that it does not include temperature effects. To address this issue we construct a coarse-grained Helmholtz free energy that is based on both the Cauchy-Born rule and the quasiharmonic assumption. The expressions for the stress and the specific heat are derived from the free energy, and the finite element (FE) method is used to form the discrete coupled thermomechanical equations.

Another key issue in multiscale computation is the boundary condition at the coarse scale/fine scale interface. The high frequency waves coming out of the fine scale region must be absorbed to prevent spurious phonon reflections. This is crucial for the temperature to be corrected. Existing approaches are based on the generalized Langevin equation[22–24] and variational principles.[25,26] In previous works[27,28] we have proposed to use the perfectly matched layer (PML), an absorbing boundary condition, to solve the problem. The PML is constructed for the atomistic structure and is designed to absorb the high frequency part, or the fine

[a)]Electronic mail: shaofan@berkeley.edu

scale part of waves. We have shown that the PML is effective for multiscale computation, and we use it again in our multiscale framework.

This paper is organized in the following way. In Sec. II we outline the proposed multiscale framework. In Secs. III and IV we discuss in detail the coarse scale model and the fine scale model. We also discuss the PML briefly in Sec. IV. The multiscale computational algorithm and a few numerical examples are presented in Sec. V. We then conclude the presentation by making a few remarks.

II. THE BASIC FRAMEWORK

The starting point of the proposed multiscale method is the following decomposition of the displacement field into a coarse scale part and a fine scale part:

$$\mathbf{u}(\mathbf{x}) = \bar{\mathbf{u}}(\mathbf{x}) + \mathbf{u}'(\mathbf{x}). \tag{1}$$

In this paper, we use the symbol to denote coarse scale quantities and the symbol $'$ for their fine scale counterparts.

We assume that $\mathbf{u}$ can be fully resolved at the atomistic level, i.e., it becomes the atomistic displacement at discrete atomic sites,

$$\mathbf{u}(\mathbf{x}) \rightarrow \mathbf{q}_i, \quad \forall\, \mathbf{x} = \mathbf{x}_i, \quad i = 1, \ldots, N,$$

where $\mathbf{x}_i$ is the position vector of atom i and $\mathbf{q}_i$ is the corresponding displacement vector. While at the continuum level, we can resolve the coarse scale component $\bar{\mathbf{u}}$; the fine scale part $\mathbf{u}'$ at this level is unresolvable.

The basic philosophy of our concurrent multiscale computational model is as follows. For a general problem, we build a coarse scale model over the *whole domain*, by which we can obtain $\bar{\mathbf{u}}$. For some specific regions where we are interested in atomistic level details, we build fine scale models in them. Together with the coarse scale model, the fine scale model leads us to obtain $\mathbf{u}$ or $\mathbf{q}_i$. The difference between this framework and many other multiscale models is that our fine scale model alone cannot provide everything. It has to be combined with the coarse scale model. Other than "coarse scale" and "fine scale," we also use the words of "coarse region" and "fine region." Since our coarse scale model exists everywhere, a coarse region denotes a region where no fine scale model is present, while a fine region is where both the fine scale and coarse scale models exist. We have mentioned the PML in Sec. I. The PMLs are appended to fine regions. Physically fictitious, they are used to absorb high frequency waves coming out of fine regions.

The conceptual picture of our multiscale framework is illustrated in Figs. 1 and 2. By constructing a ubiquitous coarse scale model and complementing it with fine scale models, the framework fits well with the multiscale concept [Eq. (1)]. It also has some appealing features. For example, it is very easy to build an adaptive multiscale model under this framework: fine scale models can be constructed and removed based on coarse scale level error estimates.

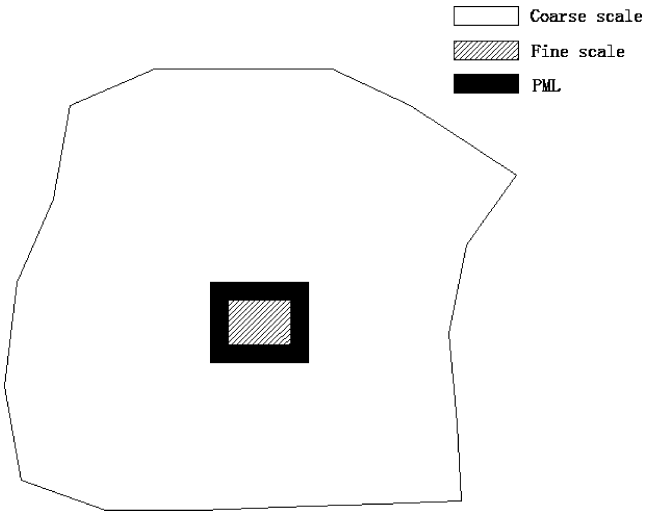

FIG. 1. A domain with different regions of required resolutions.

III. THE COARSE SCALE MODEL

Our course scale model is based on a coarse-grained Helmholtz free energy. The theory, which is based on the Cauchy-Born rule and quasiharmonic approximation, is stated in textbooks.[29] A few authors have utilized the idea in various applications.[30–32] We shall use the coarse-grained free energy to derive macroscopic quantities in coupled thermomechanical equations.

Let us consider a general three dimensional (3D) lattice which contains N atoms. For the sake of simplicity, we consider the case in which the unit cell of the lattice has only one atom. The domain is denoted by Ω_e. The reference and current positions of the atoms are denoted as $\mathbf{X}_i$ and $\mathbf{x}_i$, respectively. At finite temperature, the atoms vibrate around $\mathbf{x}_i$, and the displacement with respect to $\mathbf{x}_i$ is $\mathbf{u}_i$. Let $\mathbf{q}_i = \mathbf{x}_i + \mathbf{u}_i$. If we assume the deformation in Ω_e to be homogeneous, then we have the following equation:

$$\mathbf{a}_i = \mathbf{F}^e \mathbf{a}_i^0, \quad i = 1,2,3, \tag{2}$$

where $\mathbf{a}_i$ and $\mathbf{a}_i^0$ are basis vectors for the deformed and original lattices, respectively. $\mathbf{F}^e$ is the deformation gradient.

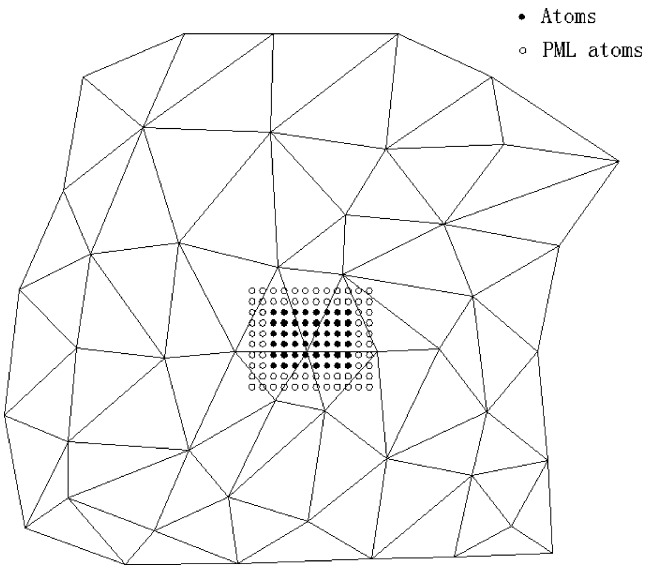

FIG. 2. A domain with different physical modelings.

Equation (2) is called the Cauchy-Born rule.[33] In practice, this finite lattice is embedded into a (linear) finite element.

If we only consider nearest neighbor interactions, U_0, the potential energy of the deformed lattice with all atoms resting in their current positions without thermal vibration can be written as

$$U_0 = \sum_{i=1}^{N} \sum_{j=i+1}^{N} \varphi(r^{ij}), \tag{3}$$

where φ is the potential function between a pair of atoms and r^{ij} is the distance between atoms i and j. In the case of homogeneous deformation, the interactions along the direction of $\mathbf{a}_1$, $\mathbf{a}_2$, or $\mathbf{a}_3$ are the same. U_0 can be written as

$$U_0 = N_{p1}\varphi(|\mathbf{a}_1|) + N_{p2}\varphi(|\mathbf{a}_2|) + N_{p3}\varphi(|\mathbf{a}_3|), \tag{4}$$

where N_{pi} is the number of nearest neighbor pairs in ith direction.

There is no difficulty to extend the above discussion to more general cases with multibody interactions and many-atom unit cells. We will have the following general result:

$$U_0 = U_0(\mathbf{F}^e). \tag{5}$$

It is noted that the evaluation of U_0 takes less time. This is because of assumption of homogeneous deformation, and we do not need to calculate every interaction to compute U_0.

Under the theory of quantum mechanics, the Helmholtz free energy has the form of[29]

$$\mathcal{F}(\mathbf{F}^e, T) = U_0(\mathbf{F}^e) + k_B T \sum_{i=1}^{N} \log\left[2\sinh\left(\frac{\hbar\omega_i(\mathbf{a}(\mathbf{F}^e))}{4\pi k_B T}\right)\right], \tag{6}$$

where $\mathbf{a}=\{\mathbf{a}_1,\mathbf{a}_2,\mathbf{a}_3\}$, T is the temperature, k_B is the Boltzmann constant and $\hbar$ is Planck's constant divided by 2π. ω_i are normal mode frequencies for the lattice. They depend on $\mathbf{F}^e$ through $\mathbf{a}_i$. It is possible to compute ω_i for some simple type of lattices, e.g., a one-dimensional lattice with identical atoms and quadratic potentials. For a general 3D lattice, one simple way to compute ω_i is to adopt the local harmonic approximation,[32]

$$\left| m\omega_{ik}^2 \mathbf{I} - \frac{\partial^2 U_0}{\partial \mathbf{x}_i \partial \mathbf{x}_i} \right| = 0, \quad i = 1, \ldots, N, \tag{7}$$

where ω_{ik} are the three frequencies for atom i. In general, the frequencies are functions of the deformation gradient.

With $\mathcal{F}$ available, we can derive the expression for entropy S,

$$S = -\frac{\partial \mathcal{F}}{\partial T} = \frac{k_B}{T}\sum_i \left(\frac{\hbar\omega_i(\mathbf{F}^e)}{4\pi k_B}\right)\coth\left(\frac{\hbar\omega_i(\mathbf{F}^e)}{4\pi k_B T}\right) - \frac{k_B}{T}\sum_i \log\left[2\sinh\left(\frac{\hbar\omega_i(\mathbf{F}^e)}{4\pi k_B T}\right)\right] \tag{8}$$

and the internal energy E,

$$E = \mathcal{F} + TS = U_0 + k_B \sum_i \left(\frac{\hbar\omega_i(\mathbf{F}^e)}{4\pi k_B}\right)\coth\left(\frac{\hbar\omega_i(\mathbf{F}^e)}{4\pi k_B T}\right). \tag{9}$$

The governing equations at the coarse scale level are the equilibrium equation and the first law of thermodynamics. The former is written as

$$\operatorname{div}\mathbf{P} + \rho_0\mathbf{B} = \rho_0\ddot{\mathbf{x}}, \tag{10}$$

where $\mathbf{P}$ is the first Piola-Kirchhoff stress, ρ_0 is the density in material configuration, and $\mathbf{B}$ is the body force and div is the material divergence operator.

The equation of thermodynamic first law can be expressed as[34]

$$\dot{w} = \rho_0 z - \operatorname{div}\mathbf{Q} + \mathbf{P}\cdot\dot{\mathbf{F}}^e, \tag{11}$$

where ρ_0 is the density, w is the internal energy per unit reference volume, z is the heat source per unit mass, and $\mathbf{Q}$ is the heat flux. The left hand side can be written as

$$\dot{w} = \frac{E}{V^e} = \frac{1}{V^e}\frac{\partial E}{\partial \mathbf{F}^e}\cdot\dot{\mathbf{F}}^e + \frac{1}{V^e}\frac{\partial E}{\partial T}\dot{T} = \frac{1}{V^e}\frac{\partial \mathcal{F}}{\partial \mathbf{F}^e}\cdot\dot{\mathbf{F}}^e + \frac{T}{V^e}\frac{\partial S}{\partial \mathbf{F}^e}\cdot\dot{\mathbf{F}}^e + \frac{1}{V^e}\frac{\partial E}{\partial T}\dot{T}. \tag{12}$$

If we define

$$\mathbf{P} = \frac{1}{V^e}\frac{\partial \mathcal{F}}{\partial \mathbf{F}^e}, \tag{13}$$

$$\mathbf{C}_T = T\frac{\partial S}{\partial \mathbf{F}^e} = -T\frac{\partial^2 \mathcal{F}}{\partial T \partial \mathbf{F}^e}, \tag{14}$$

$$C_V = \frac{\partial E}{\partial T} = T\frac{\partial^2 \mathcal{F}}{\partial T^2}, \tag{15}$$

then Eq. (12) can be rewritten as

$$\dot{w} = \mathbf{P}\cdot\dot{\mathbf{F}}^e + \frac{\mathbf{C}_T}{V^e}\cdot\dot{\mathbf{F}}^e + \frac{C_V}{V^e}\dot{T}. \tag{16}$$

Equations (13)–(15) are thermomechanical definitions of the stress, the specific heat at constant temperature, and the specific heat at constant volume.

For the heat flux $\mathbf{Q}$, we exploit the Fourier law,

$$\mathbf{Q} = -\kappa_T \nabla T, \tag{17}$$

where κ_T is the thermal conductivity.

The final expression for the first law is obtained by substituting Eqs. (16) and (17) into Eq. (11),

$$\frac{\mathbf{C}_T}{V^e}\cdot\dot{\mathbf{F}}^e + \frac{C_V}{V^e}\dot{T} = \rho_0 z + \kappa_T \nabla^2 T. \tag{18}$$

The derivation for the left hand side is now complete.

The expressions for $\mathbf{P}$, $\mathbf{C}_T$, and C_V can all be derived from the Helmholtz free energy $\mathcal{F}$. They are listed below.

$$\mathbf{P}^e(\mathbf{F}^e,T)=\frac{1}{V_e}\frac{\partial \mathcal{F}}{\partial \mathbf{F}^e}=\frac{1}{V_e}\left\{U_0'(\mathbf{F}^e)+\frac{\hbar}{4\pi}\sum_{i=1}^{N}\left[\coth\left(\frac{\hbar\omega_i(\mathbf{F}^e)}{4\pi k_B T}\right)\omega_i'(\mathbf{F}^e)\right]\right\}, \tag{19}$$

$$C_V(\mathbf{F}^e,T)=T\frac{\partial^2 \mathcal{F}}{\partial T^2}=k_B\sum_i\left(\frac{\hbar\omega_i(\mathbf{F}^e)}{4\pi k_B T}\right)^2\cdot\frac{1}{\sinh^2(\hbar\omega_i(\mathbf{F}^e)/4\pi k_B T)}, \tag{20}$$

$$\mathbf{C}_T(\mathbf{F}^e,T)=-T\frac{\partial^2 \mathcal{F}}{\partial T\partial \mathbf{F}^e}=\frac{-\hbar^2}{16\pi^2 k_B T}\frac{\omega(\mathbf{F}^e)\omega'(\mathbf{F}^e)}{\sinh^2(\hbar\omega_i(\mathbf{F}^e)/4\pi k_B T)}. \tag{21}$$

For the thermal conductivity κ_T, we exploit the result from the kinetic theory,[35]

$$\kappa_T=\tfrac{1}{3}C_V v\ell, \tag{22}$$

where C_V is the heat capacity, v is the average particle velocity, and ℓ is the particle mean free path. For metals, we have

$$\ell=v_F\tau, \tag{23}$$

where v_F is the Fermi surface velocity and τ is the collision time. The values of both v_F and τ can be obtained from standard references, e.g., Ref. 37. Since we already have the expression for $C_V=C_V(\mathbf{F}^e,T)$, we can write κ_T as

$$\kappa_T=\kappa_T(\mathbf{F}^e,T).$$

Up to now, we have derived the expressions for $\mathbf{P}$, $\mathbf{C}_T$, C_V, and κ_T, and all of them can be expressed as functions of $\mathbf{F}^e$ and T. This facilitates our goal to use the FE method to discretize the domain. The procedures to obtain FE equations are as follows. We need the weak forms of Eqs. (10) and (18), which are written as

$$\int_{\Omega_0}\rho_0\ddot{\mathbf{x}}\cdot\delta\mathbf{u}dV+\int_{\Omega_0}\mathbf{P}\cdot\delta\mathbf{F}dV=\int_{\partial\Omega_0}\bar{\mathbf{t}}\cdot\delta\mathbf{u}dS, \tag{24}$$

$$\int_{\Omega_0}\frac{C_V}{\Omega_0}\dot{T}\delta T dV+\int_{\Omega_0}\frac{\mathbf{C}_T}{\Omega_0}\cdot\dot{\mathbf{F}}\delta T dV+\int_{\Omega_0}\kappa_T\nabla T\cdot\nabla\delta T dV=\int_{\Omega_0}\rho_0 z\delta T dV+\int_{\partial\Omega_0}\bar{\mathbf{Q}}\cdot\nabla\delta T dS, \tag{25}$$

where $\bar{\mathbf{t}}$ and $\bar{\mathbf{Q}}$ are given traction and heat flux at the boundary.

The referential domain Ω_0 is then broken into a set of elements $\{\Omega_e\}, e=1,\ldots,Ne$. The integrals in Eqs. (24) and (25) are expressed as summations of integrals over Ω_e. The coarse scale displacement $\bar{\mathbf{u}}$ and temperature T are approximated by interpolation,

$$\bar{\mathbf{u}}\approx\mathbf{N}_u\mathbf{d}, \tag{26}$$

$$T\approx\mathbf{N}_T\mathbf{T}, \tag{27}$$

where $\mathbf{N}_u$ and $\mathbf{N}_T$ are shape function matrices[36,37] for $\bar{\mathbf{u}}$ and T. $\mathbf{d}$ and $\mathbf{T}$ are nodal displacement and temperature vectors. It is easy to obtain that

$$\mathbf{F}=\frac{\partial\mathbf{x}}{\partial\mathbf{X}}=\mathbf{1}+\frac{\partial\bar{\mathbf{u}}}{\partial\mathbf{X}}=\mathbf{1}+\mathbf{B}_u\mathbf{d}, \tag{28}$$

where $\mathbf{B}_u$ is the shape function derivative matrix for displacement. So $\mathbf{F}$ is a function of $\mathbf{d}$. Thus $\mathbf{P}$, $\mathbf{C}_T$, C_V, and κ_T are functions of $\mathbf{d}$ and $\mathbf{T}$ with the FE approximation.

The final form of FE equations are

$$\mathbf{M}\ddot{\mathbf{u}}=\mathbf{f}^{ext}-\mathbf{f}^{\text{int}} \tag{29}$$

$$\mathbf{C}_V\dot{\mathbf{T}}+\mathbf{C}_T\dot{\mathbf{u}}+\mathbf{K}_T\mathbf{T}=\mathbf{h}^{\text{body}}+\mathbf{h}^{\text{boun}} \tag{30}$$

The matrices and vectors are

$$\mathbf{M}=\mathop{A}_{e}\int_{\Omega^e}\rho_0\mathbf{N}_u^{eT}\mathbf{N}_u^e dX, \tag{31}$$

$$\mathbf{f}^{\text{int}}(\mathbf{d},\mathbf{T})=\mathop{A}_{e}\int_{\Omega^e}\mathbf{B}_u^{eT}\mathbf{P}^e(\mathbf{d}^e,\mathbf{T}^e)dX, \tag{32}$$

$$\mathbf{C}_V(\mathbf{d},\mathbf{T})=\mathop{A}_{e}\int_{\Omega^e}\frac{C_v(\mathbf{d}^e,\mathbf{T}^e)}{V^e}\mathbf{N}_T^{eT}\mathbf{N}_T^e dX,$$

$$\mathbf{C}_T(\mathbf{d},\mathbf{T})=\mathop{A}_{e}\int_{\Omega^e}\frac{\mathbf{C}_T^e(\mathbf{d}^e,\mathbf{T}^e)}{V^e}\mathbf{N}_T^{eT}\mathbf{B}_u^e dX,$$

$$\mathbf{K}_T(\mathbf{d},\mathbf{T})=\mathop{A}_{e}\int_{\Omega^e}\kappa_T(\mathbf{d}^e,\mathbf{T}^e)\mathbf{B}_T^{eT}\mathbf{B}_T^e dX,$$

$$\mathbf{h}^{\text{body}}=\mathop{A}_{e}\int_{\Omega^e}\rho_0 z\mathbf{N}_T^{eT}dX,$$

$$\mathbf{h}^{\text{boun}}=\mathop{A}_{e}\int_{\partial\Omega^e}\mathbf{B}_T^{eT}\bar{\mathbf{Q}}dS, \tag{33}$$

where $\boldsymbol{A}$ is the assembly operator.[36] Equations (29) and (30) are nonlinear coupled equations for nodal unknowns $\mathbf{d}$ and $\mathbf{T}$.

In coarse regions we solve Eqs. (29) and (30) to obtain $\bar{\mathbf{u}}$ and T. In fine regions we want to take advantage of the additional information available, which is the atomistic position $\mathbf{q}$ obtained through the fine scale model. The internal force vector $\mathbf{f}^{\text{int}}$ is then obtained by mapping the atomistic force vector $\mathbf{F}$ to nodes. Similarly, in fine regions we use the values of fine scale atomistic velocities to update coarse scale temperatures. By doing so, the coarse scale model is coupled with the fine scale model.

IV. THE FINE SCALE MODEL

As discussed in Sec. I, we should view the coarse scale quantities as the mean field and the fine scale quantities as

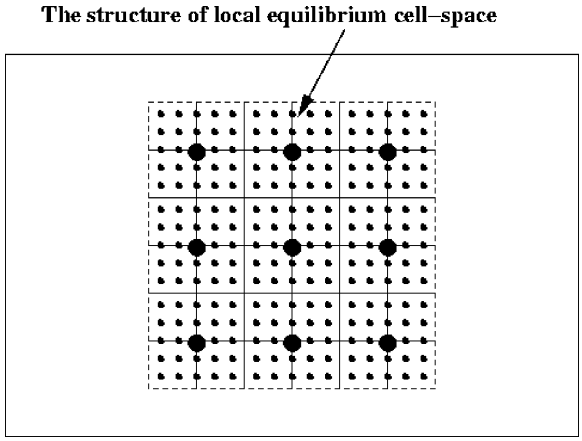

FIG. 3. Illustration of the finite-element nodal ensemble.

the fluctuation. The goal of our fine scale model, which is built at the atomistic level, is to compute the fluctuations.

From Eq. (1), we have the decomposition for velocities,

$$\mathbf{v} = \bar{\mathbf{v}} + \mathbf{v}'. \tag{34}$$

We claim that only the fine scale part of the momentum contributes to the kinetic temperature,

$$\frac{3}{2}Nk_BT = \left\langle \sum_i \frac{\mathbf{p}_i' \cdot \mathbf{p}_i'}{2m_i} \right\rangle, \tag{35}$$

where $<\cdot>$ denotes averaging in time.

In the classical concept of a thermal reservoir, an NVT ensemble is embedded into an infinitely large thermal reservoir, whose temperature remains constant during an equilibrium process. For our multiscale model, we argue that in an equilibrium process the coarse scale may be viewed as a "*coarse scale reservoir*" since temperature is a macroscopic or coarse scale quantity. Under this concept, each coarse scale node represents a reservoir and governs a set of atoms (see Fig. 3 for an illustration). We call these subsets of atoms nodal sets and the replica of these subsets in the phase space nodal ensembles, and we call the collection of nodal ensembles the *multiscale ensemble*.

For a nonequilibrium process the same concept can be applied if we adopt the local thermodynamic equilibrium postulate, which is widely used in nonequilibrium thermodynamics.[9] To apply the postulate to our multiscale model, we argue that the temperature of each coarse scale nodal reservoir remains constant within each coarse scale time step. Thus without external fields, the atoms of a nodal set are assumed to be in a equilibrium state within one coarse scale time step.

What raises the question mark is the fact that the nodal sets of atoms are not isolated to each other. They are open subsystems with flux exchange from each other. Although we belive that the these subsystems are very closed to equilibrium within one coarse scale time step, the validity of the local equilibrium postulate remains to be verified.

While the coarse scale mean fields are decided by the coarse scale model, they act on the fine scale model as external fields. The idea of including the effect of macroscopic quantities to the atomistic model has long been established by NEMD researchers. For example, in the DOLLS (Ref. 14) and SLLOD (Ref. 15) algorithms designed to simulate Couette flow the shear strain rate is included as an external field. In our fine scale model the coarse scale velocities and accelerations are treated as external fields.

We propose that our fine scale adiabatic EOM for one particular nodal set can be derived from the following Hamiltonian:

$$H^{\text{adia}}(\mathbf{q},\mathbf{p}') = \sum_i^{N_e} \frac{1}{2m_i}\mathbf{p}_i' \cdot \mathbf{p}_i' + U(\mathbf{q}) + \sum_i^{N_e} \frac{1}{m_i}\bar{\mathbf{p}}_i \cdot \mathbf{p}_i' + \sum_i^{N_e} \dot{\bar{\mathbf{p}}}_i \cdot \mathbf{q}_i, \tag{36}$$

where N_e is the number of atoms in the nodal set e. Our unknowns are total scale position $\mathbf{q}$ and fine scale momentum $\mathbf{p}'$. At each atom the coarse scale momenta $\bar{\mathbf{p}}_i$ and forces $\dot{\bar{\mathbf{p}}}_i$ are obtained by interpolating nodal values. The equations of motion are

$$\dot{\mathbf{q}}_i = \frac{\partial H^{\text{adia}}}{\partial \mathbf{p}_i'} = \frac{\mathbf{p}_i'}{m_i} + \frac{\bar{\mathbf{p}}_i}{m_i}, \tag{37}$$

$$\dot{\mathbf{p}}_i' = -\frac{\partial H^{\text{adia}}}{\partial \mathbf{q}_i} = \mathbf{F}_i - \dot{\bar{\mathbf{p}}}_i. \tag{38}$$

The above equations are nothing but decompositions of atomistic velocity and acceleration.

Remark 4.1: *The physical interpretation of the term* $\Sigma_i \dot{\bar{\mathbf{p}}}_i \cdot \mathbf{q}_i$ *in* H^{adia} *can be seen as follows:*

$$\dot{\bar{\mathbf{p}}}_i = -\mathbf{f}^{\text{int}}(\mathbf{x}_i), \tag{39}$$

where $\mathbf{f}^{\text{int}}$ *is the coarse scale internal force. So*

$$\sum_i \dot{\bar{\mathbf{p}}}_i \cdot \mathbf{q}_i = -\sum_i \mathbf{f}^{\text{int}}(\mathbf{x}_i) \cdot \mathbf{q}_i \approx -\int_{\Omega_e} \mathbf{f}^{\text{int}} \cdot \mathbf{u} d\mathbf{x}. \tag{40}$$

We assume that the work done by coarse scale internal force on fine scale displacements is zero,

$$\int_{\Omega_e} \mathbf{f}^{\text{int}} \mathbf{u}' d\mathbf{x} = 0. \tag{41}$$

This assumption is valid if we view $\mathbf{u}'$ *as fluctuations. With Eq. (41) we obtain*

$$\sum_i \dot{\bar{\mathbf{p}}}_i \cdot \mathbf{q}_i = -\int_{\Omega_e} \mathbf{f}^{\text{int}} \mathbf{u} d\mathbf{x} = -\int_{\Omega_e} \mathbf{f}^{\text{int}} \bar{\mathbf{u}} d\mathbf{x} = -\bar{U}. \tag{42}$$

So $\Sigma_i \dot{\bar{\mathbf{p}}}_i \cdot \mathbf{q}_i$ *represents the negative coarse scale potential energy. Now if we define a coarse scale Hamiltonian,*

$$\bar{H} = \bar{K} + \bar{U} = \sum_i \frac{1}{2m_i}\bar{\mathbf{p}}_i \cdot \bar{\mathbf{p}}_i + \bar{U}, \tag{43}$$

then we have

$$H^{\text{adia}} + \bar{H} = \sum_i^{N_e} \frac{1}{2m_i}\mathbf{p}_i' \cdot \mathbf{p}_i' + \sum_i^{N_e} \frac{1}{m_i}\bar{\mathbf{p}}_i \cdot \mathbf{p}_i' + \sum_i \frac{1}{2m_i}\bar{\mathbf{p}}_i \cdot \bar{\mathbf{p}}_i + U(\mathbf{q}) = K + U = H^{\text{total}}, \tag{44}$$

where H^{total} is the total energy. So H^{adia} represents the fine scale energy.

As previously discussed, the temperature of a nodal set is decided at the coarse scale level. To maintain the fine scale model in a steady state, thermostats need to be added to the model. Similar to NEMD, constant temperature MD is a well-studied subject. Among different approaches, we are interested in reversible and deterministic thermostats. Among them, the Gaussian thermostat[38,39] aims to preserve the system's (fine scale) kinetic energy. The Nosé-Hoover (NH) thermostat[40,41] tries to make the time average in the thermostated system equivalent to the ensemble average in a constant temperature system. The Nosé-Hoover chain (NHC) thermostat[42] extends the NH thermostat by using a chain of thermostat variables. At equilibrium it can be proven[9] that both NH and NHC thermostats can reproduce a canonical distribution, while the Gaussian thermostat can achieve the same goal in the thermodynamic limit, and the NHC thermostat outperforms the NH thermostat for stiff systems. The Gaussian thermostat can be easily extended to nonequilibrium cases, while both NH and NHC thermostats experience setbacks when the system is far from equilibrium.[43–46] We choose to adopt the NHC thermostat in our fine scale model because it is easier to handle a varying temperature. With the local equilibrium postulate, we expect the system to stay in the range where the NHC thermostat performs well. In practice we found satisfactory temperature control. The numerical results are shown in Sec. 5. Adoption of the Gaussian thermostat and the comparison between different thermostats will be explored in the future.

With the NHC thermostat, the equations of motion become

$$\dot{\mathbf{q}}_i = \frac{\mathbf{p}_i'}{m_i} + \frac{\bar{\mathbf{p}}_i}{m_i}, \tag{45}$$

$$\dot{\mathbf{p}}_i' = \mathbf{F}_i - \dot{\bar{\mathbf{p}}}_i - \xi_1 \mathbf{p}_i', \tag{46}$$

$$\dot{\xi}_1^e = \frac{1}{Q_1}\left(\sum_i \frac{1}{m_i}\mathbf{p}_i' \cdot \mathbf{p}_i' - 3Nk_BT^e\right) - \xi_2^e\xi_1^e, \tag{47}$$

$$\dot{\xi}_j^e = \frac{1}{Q_j}(Q_{j-1}\xi_{j-1}^{e\,2} - k_BT^e) - \xi_{j+1}^e\xi_j^e,$$

$$j = 2, \ldots, M-1 \tag{48}$$

$$\dot{\xi}_M^e = \frac{1}{Q_M}(Q_{M-1}\xi_{M-1}^{e\,2} - k_BT^e), \tag{49}$$

where $\{\xi_j^e\}$ are a chain of thermostat variables for nodal set e and Q_j are parameters associated with them. M is the length of the NHC. T^e is the temperature for nodal set e. Equations (45)–(49) cannot be derived from a Hamiltonian. But the following internal energy is conserved:[47]

$$H^{\text{NHC}}(\mathbf{q},\mathbf{p}',\boldsymbol{\xi}) = \sum_i^{N_e} \frac{1}{2m_i}\mathbf{p}_i' \cdot \mathbf{p}_i' + \sum_i^{N_e} \frac{1}{m_i}\bar{\mathbf{p}}_i \cdot \mathbf{p}_i' + U(\mathbf{q}) + \sum_i^{N_e} \dot{\bar{\mathbf{p}}}_i \cdot \mathbf{q}_i + \sum_{j=1}^{M} \frac{\xi_j^2}{2Q_j} + 3Nk_BT^e\xi_1 + \sum_{j=2}^{M} k_BT^e\xi_j. \tag{50}$$

Now we want to show that the equations of motion [Eqs. (45)–(49)] generate the correct thermodynamics. The quantity we want to study is f, the probability distribution function of the phase space. For simplicity, the following discussion is sketched based on the NH thermostat instead of the NHC thermostat. However, since the NHC thermostat is an extension to the NH thermostat, all the conclusions can be obtained for the NHC thermostat without fundamental differences. With the NH thermostat, $\xi_2^e = 0$ in Eq. (47) and we do not have Eqs. (48) and (49). Our domain of interest is a nodal set e. All superscripts e are dropped to make the expressions less cumbersome.

The distribution f defines the density of points in the phase space.[48] It is a function of time and phase space variables, which are $\mathbf{q}$, $\mathbf{p}'$, and ξ_1 in our NH thermostated fine scale model. Since the atoms in nodal set e have the same temperature, f should be canonical,[48]

$$f(\mathbf{q},\mathbf{p}',\xi_1,t) = C\exp[-\beta H_0(\mathbf{q},\mathbf{p}')] \times g(\xi_1) \times h(t), \tag{51}$$

where

$$H_0(\mathbf{q},\mathbf{p}') = \sum_i \frac{1}{2m_i}\mathbf{p}_i' \cdot \mathbf{p}_i' + U(\mathbf{q}). \tag{52}$$

In Eq. (51) the exponential term is the canonical distribution function for $\mathbf{q}$ and $\mathbf{p}'$. $g(\xi_1)$ is the distribution function for ξ_1 and $h(t)$ represents the coarse scale contributions.

Now we want to see whether or not we can obtain such type of distribution functions. The starting point is the well-known Liouville equation,

$$\frac{df}{dt} = -f\left(\frac{\partial}{\partial \mathbf{q}} \cdot \dot{\mathbf{q}} + \frac{\partial}{\partial \mathbf{p}'} \cdot \dot{\mathbf{p}}' + \frac{\partial}{\partial \xi_1}\dot{\xi}_1\right). \tag{53}$$

From Eqs. (45)–(47) we can easily obtain

$$\frac{df}{dt} = 3N_e\xi_1 f. \tag{54}$$

Now we consider the following pseudoenergy measure:

$$H_0^* = \sum_i \frac{1}{2m_i}\mathbf{p}_i' \cdot \mathbf{p}_i' + \sum_i \frac{1}{2m_i}\bar{\mathbf{p}}_i \cdot \bar{\mathbf{p}}_i + U(\mathbf{q}). \tag{55}$$

We want to compute $(d/dt)H_0^*$, which is carried as follows:

$$\frac{d}{dt}H_0^* = \sum_i \left(\frac{1}{m_i}\dot{\mathbf{p}}_i' \cdot \mathbf{p}_i' + \frac{1}{m_i}\dot{\bar{\mathbf{p}}}_i \cdot \bar{\mathbf{p}}_i - \mathbf{F}_i \cdot \dot{\mathbf{q}}_i \right)$$

$$= \sum_i \frac{-1}{m_i}(\mathbf{p}_i' \cdot \dot{\bar{\mathbf{p}}}_i + \xi_1 \mathbf{p}_i' \cdot \mathbf{p}_i' + \bar{\mathbf{p}}_i \cdot \dot{\mathbf{p}}_i' + \xi_1 \bar{\mathbf{p}}_i \cdot \mathbf{p}_i')$$

$$= -\xi_1 \left(\sum_i \frac{1}{m_i}\mathbf{p}_i' \cdot \mathbf{p}_i' \right) - \xi_1 \left(\sum_i \frac{1}{m_i}\mathbf{p}_i' \cdot \bar{\mathbf{p}}_i \right)$$

$$- \frac{d}{dt}\left(\sum_i \frac{1}{m_i}\mathbf{p}_i' \cdot \bar{\mathbf{p}}_i \right). \tag{56}$$

Both Eqs. (45) and (46) are used to obtain the above result. Inspecting Eq. (56), we find that if the following equation holds:

$$\sum_i \frac{1}{m_i}\mathbf{p}_i' \cdot \bar{\mathbf{p}}_i = 0, \tag{57}$$

we can obtain

$$\dot{H}_0^* = -\xi_1 \left(\sum_i \frac{1}{m_i}\mathbf{p}_i' \cdot \mathbf{p}_i' \right). \tag{58}$$

If we assume Eq. (57) is true, combining Eqs. (47) and (58) yields

$$\frac{d}{dt}\left(H_0^* + \frac{1}{2}Q\xi_1^2 \right) = \dot{H}_0^* + Q\xi_1\dot{\xi}_1 = -3N^e k_B T^e \xi_1. \tag{59}$$

By recalling Eq. (54), we obtain

$$\frac{d}{dt}\log f = 3N^e\xi_1 = -\beta\frac{d}{dt}\left(H_0^* + \frac{1}{2}Q\xi_1^2 \right). \tag{60}$$

We can then solve for f,

$$f(\mathbf{q},\mathbf{p}',\xi_1,t) = C\exp\left[-\beta\left(H_0^* + \frac{1}{2}Q\xi_1^2 \right) \right]$$

$$= C\exp\left[-\beta\left(H_0 + \bar{K} + \frac{1}{2}Q\xi_1^2 \right) \right]. \tag{61}$$

So for one nodal set the distribution function is indeed canonical. This conclusion is based on Eq. (57), which has not been justified. Equation (57) can be rewritten as

$$\sum_i \frac{1}{m_i}\mathbf{p}_i' \cdot \bar{\mathbf{p}}_i = \mathbf{p}' \cdot \bar{\mathbf{v}} = \mathbf{v}' \cdot \bar{\mathbf{p}} = 0, \tag{62}$$

where $\mathbf{p}'$, $\mathbf{v}'$, $\bar{\mathbf{p}}$, and $\bar{\mathbf{v}}$ are fine scale momentum, fine scale velocity, coarse scale momentum, and coarse scale velocity vector of all atoms in Ω_e, respectively. So Eq. (57) represents the orthogonality between fine scale momentum and coarse scale velocity vectors. It means that the total scale kinetic energy is decoupled in terms of $\bar{\mathbf{p}}$ and $\mathbf{p}'$.

For the present formulation, we are not able to prove that Eq. (57) holds. However, it holds in other multiscale models such as the bridging scale method.[49,50] We have constructed another multiscale formulation with a complete multiscale Hamiltonian formulation that can also generate nonlocal canonical distribution. The detailed discussions of that algorithm will be reported in a separated paper.[51]

We now examine the problem from a different perspective. With the assumption of linear response, the distribution function can be written as[9]

$$f(\mathbf{q},\mathbf{p}',\xi_1,t) = f(\mathbf{q},\mathbf{p}',\xi_1,0) + \Delta f(\mathbf{q},\mathbf{p}',\xi_1,t). \tag{63}$$

Let us assume at time zero we have a canonical distribution function,

$$f(\mathbf{q},\mathbf{p}',\xi_1,0) = f_c = C\exp\left[-\beta\left(H_0 + \frac{1}{2}Q\xi_1^2 \right) \right]. \tag{64}$$

Then by procedures described in Ref. 9, the change of distribution function can be computed to be

$$\Delta f(\mathbf{q},\mathbf{p}',\xi_1,t) = -\beta\int_0^t ds\,\exp(-iL(t-s))\cdot\left[\sum_i \frac{1}{m_i}(\mathbf{p}_i'\dot{\bar{\mathbf{p}}}_i + \mathbf{F}_i\bar{\mathbf{p}}_i) \right] f_c, \tag{65}$$

where iL is the Liouvillean operator. Equation (65) states that the change of the distribution function is independent of the thermostat. This result assures that the NH thermostat as well as the NHC thermostat does not destroy the canonical distribution with the presence of coarse scale fields. This is a more general statement in the sense that we do not need extra conditions such as Eq. (57).

With the understanding of properties of the distribution function, we conclude that the proposed fine scale model can reproduce the correct nonequilibrium thermodynamics. One point is worth explaining: In the above discussion of the distribution function, we view each nodal set as a closed system. In practice the nodal sets are connected with each other. So fluxes between nodal sets should have their contributions when we compute quantities such as $\dot{H}_0^*$. We argue that inside the whole fine scale model, i.e., the collection of nodal sets, the effect of fluxes can be omitted with the local equilibrium assumption. A more elaborated analysis will be presented in a separated paper.

We end the section with a brief discussion of the PML in our multiscale model. Please refer to Ref. 28 for a detailed study. The PML has the same lattice structure as the fine scale atomistic model. The equations of motion in the PML zone are

$$\dot{\mathbf{q}}_i = \frac{\mathbf{p}_i'}{m_i} + \frac{\bar{\mathbf{p}}_i}{m_i}, \tag{66}$$

$$\dot{\mathbf{p}}_i' = \mathbf{F}_i^{\mathrm{lin}} - \dot{\bar{\mathbf{p}}}_i + 2d_i\mathbf{p}_i' + d_i^2 m_i \mathbf{q}_i, \tag{67}$$

where $\mathbf{F}_i^{\mathrm{lin}}$ is the linearized interatomic force. The expressions for damping coefficients d_i are

$$d_i = \log\left(\frac{1}{R}\right)\frac{3v}{2L_{\mathrm{PML}}}\frac{r_{\mathrm{PML},i}^2}{L_{\mathrm{PML}}}, \tag{68}$$

where $R<1$ is a free parameter, v is the wave velocity, L_{PML} is the thickness of the PML, and $r_{\mathrm{PML},i}$ is the distance between atom i and the MD/PML interface.

V. IMPLEMENTATION AND NUMERICAL RESULTS

A pseudocode for the complete multiscale algorithm is given as follows:

(1) Start at t_I^c, with $\{\mathbf{u}_I, \dot{\mathbf{u}}_I, \ddot{\mathbf{u}}_I, \mathbf{T}_I, \dot{\mathbf{T}}_I\}$.
(2) Start at t_0^f, with $\{\mathbf{q}_{I,0}^{\mathrm{MD}}, \dot{\mathbf{q}}_{I,0}^{\mathrm{MD}}\}$ and $\{\mathbf{q}_{I,0}^{\mathrm{PML}}, \dot{\mathbf{q}}_{I,0}^{\mathrm{PML}}\}$.
(3) Set up heat reservoirs with temperatures $\mathbf{T}_I$.
(4) Do $t^f = t_0^f : t_{\mathrm{ncyl}}^f$.
(5) Solve MD equations for $\{\mathbf{q}_{I,i}^{\mathrm{MD}}, \dot{\mathbf{q}}_{I,i}^{\mathrm{MD}}, \ddot{\mathbf{q}}_{I,i}^{\mathrm{MD}}\}$ with each atom associated with a heat reservoir.
(6) Solve PML equations for $\{\mathbf{q}_{I,i}^{\mathrm{PML}}, \dot{\mathbf{q}}_{I,i}^{\mathrm{PML}}\}$.
(7) Fine scale cycle ends.
(8) Solve FE equations for $\{\mathbf{u}_{I+1}, \dot{\mathbf{u}}_{I+1}, \ddot{\mathbf{u}}_{I+1}, \mathbf{T}_{I+1}, \dot{\mathbf{T}}_{I+1}\}$.
(9) Advance to t_{I+1}^c.

We have ncyl fine scale time steps in one coarse scale time step.

The explicit central difference method is used to integrate coarse scale equations. For PML equations of motion, the velocity Verlet algorithm[47] is adopted. To integrate the fine scale equations of motion, we adopt the VV-1 algorithm described in Ref. 52. This algorithm is known to have problems for very long simulations of stiff systems.[53,54] Under the conditions of our simulations, they work fine. Nevertheless, it is definitely worthwhile to implement other algorithms for NHC dynamics, e.g., Ref. 55, for comparison purpose.

To validate the proposed coarse scale model, we examine the equilibrium distance of an atomistic system as a function of temperature in the absence of external forces. We carry out a series of simulations, in which we first start at zero temperature and then increase the temperature to a certain level. After the atoms reach their equilibrium state, we measured the equilibrium distance among atoms at this temperature by averaging the equilibrium bond lengths. For comparison, we also compute the equilibrium distance at various temperatures by minimizing the Helmholtz free energy $\mathcal{F}$. For a given potential, this minimization can be done analytically.

We choose the Morse potential with parameters for aluminum in the numerical example. The expression for the Morse potential is

$$\varphi(r^{ij}) = De^{-2\alpha(r^{ij}-r_0)} - 2De^{-\alpha(r^{ij}-r_0)}. \tag{69}$$

The parameters for aluminum are[56]

$$r_0 = 3.253\ \text{A}, \quad \alpha = 1.1646\ \text{A}^{-1}, \quad D = 0.2703\ \text{eV}, \quad \text{and } m = 26.98\ \text{amu}. \tag{70}$$

We used 100 atoms and 10 elements in the simulation. The result is shown in Fig. 4. The result obtained from the coarse-grained formulation is very close to the theoretical result.

To illustrate how the proposed multiscale model captures the thermomechanical coupling at small scale in a nonequilibrium process, we simulate a problem of one-dimensional thermostated sine-Gordon equation whose soliton solution may be interpreted as the dislocation motion. The potential energy of the system is

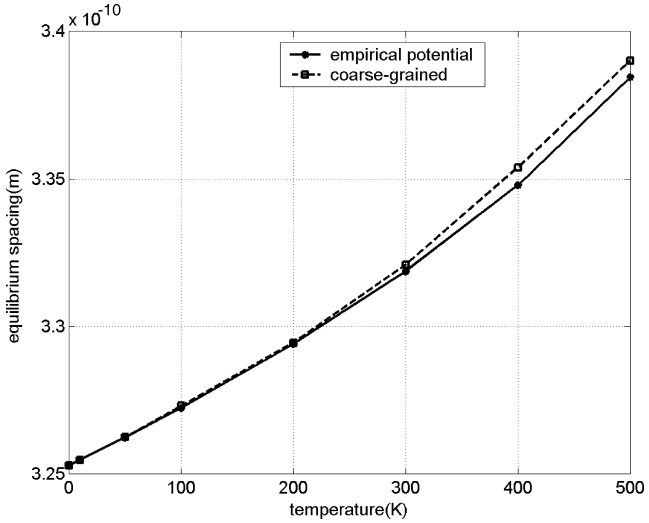

FIG. 4. Comparison of the equilibrium distance between atoms.

$$\varphi(r) = D\left[\frac{1}{2}(\alpha r)^2 + 1 - \cos(\alpha(r - r_0))\right], \tag{71}$$

where r_0 is the equilibrium distance. D, α, and r_0 are chosen as the same ones in Morse potential for aluminum. We simulate a domain of $[-300r_0, 300r_0]$ with a total of 60 FE elements. The fine scale domain is at $[-60r_0, 60r_0]$ and consists of 120 atoms. The PML at each side has 15 atoms. The coarse scale time step is 10^{-13} s and the number of subcycles per coarse scale time step is 10. We have a total of 12 thermostats. Each thermostat governs ten atoms.

We compute three cases. The first case has a uniform of 100 K initial temperature. The second case has a uniform of 10 K initial temperature. For the third case we have a 0 K initial temperature at $[-300r_0, -60r_0]$ and a 200 K initial temperature at $[60r_0, 300r_0]$. At the fine region $[-60r_0, 60r_0]$ the initial temperature varies linearly from 0 to 200 K. In all cases we have a random initial velocity. The magnitude of the velocity is adjusted so that the initial kinetic energies are 100, 10, and 100 K for the three cases. The initial displacement is set to be zero in all three cases. The length of the simulation is about 600 coarse scale time steps.

Figure 5 shows the histories of the displacement field of one-dimensional "dislocation motion" or soliton motion under different initial temperatures. For the same initial disturbance, the displacement profile for the initial temperature $T = 10$ K is almost negligible, whereas for the initial temperature $T = 100$ K one can observe the motions of solitons or dislocations. This suggests that a higher initial temperature will trigger solitons or dislocation motions. This result agrees with the observation in a similar NEMD simulation reported in Ref. 12. Furthermore, for the case (c), one may observe that the displacement waves have higher amplitude in the higher temperature region. This is another indication of the thermal activation of dislocations. The multiscale simulation results are juxtoposed with the simulation results based on the coupled thermal-mechanical macroscale formulation: Figs. 5(d)–5(f). One can find that the temperature fluctuation has significant effects on the displacement field.

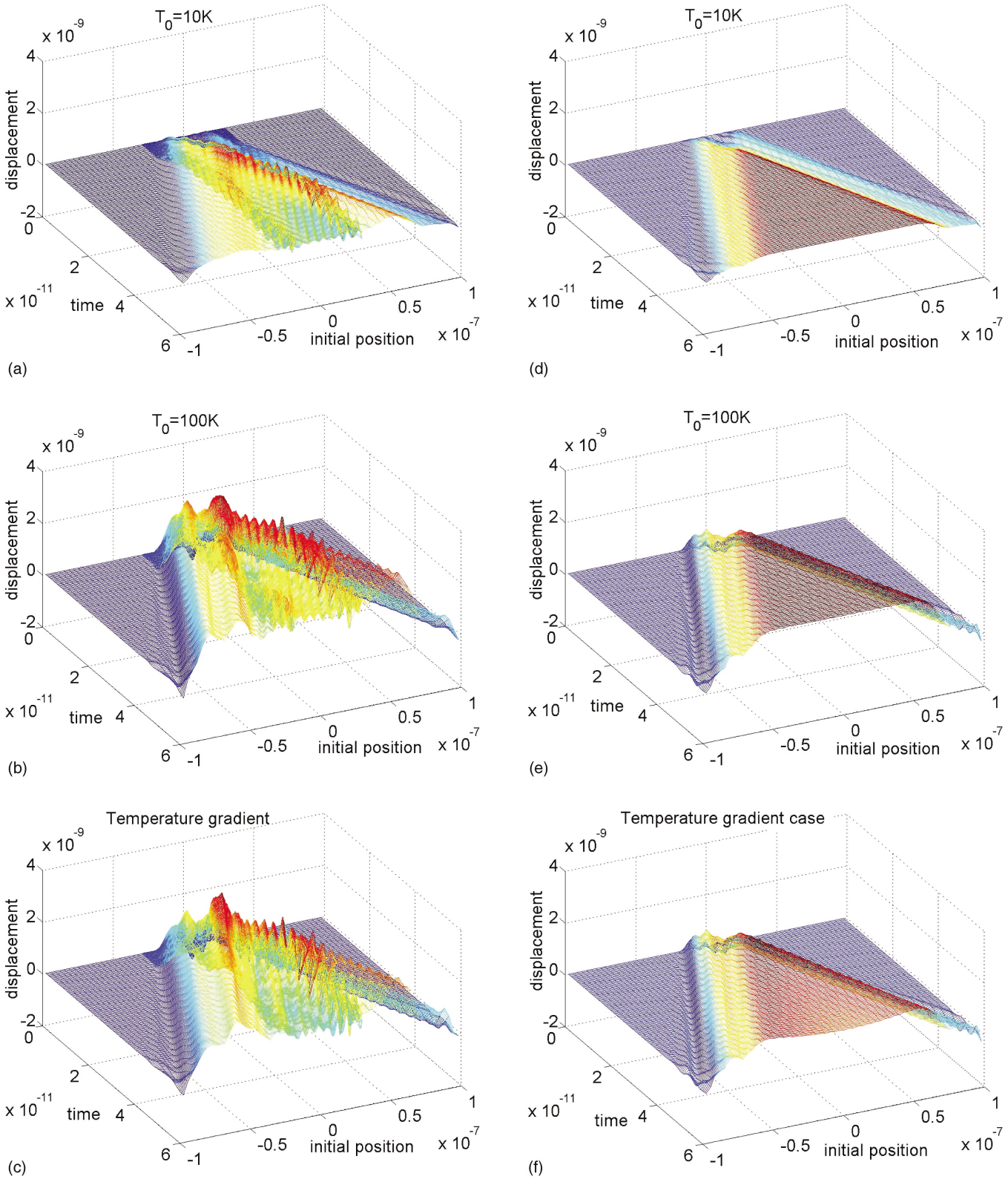

FIG. 5. (Color) Simulations of thermal activation of dislocation. (Displacement histories) Multiscale simulation: (a) $T_0=10$ K, (b) $T_0=100$ K, and (c) non-uniform initial temperature. Macroscale simulation: (d) $T_0=10$ K, (e) $T_0=100$ K, and (f) non-uniform initial temperature.

To study the thermomechanical coupling, the histories of the coarse scale temperature evolution for all three cases are shown in Figs. 6(a)–6(c). We find that in the first two cases that the dislocation motion" or the soliton propagation triggers temperature fluctuations. Such temperature fluctuation follows the dislocation motion and propagates from fine scale region to the coarse region. However, the magnitude of the fluctuation is limited to about 10% of the total temperature. For the case with a temperature gradient, we find that the temperature gradient also propagates with dislocation

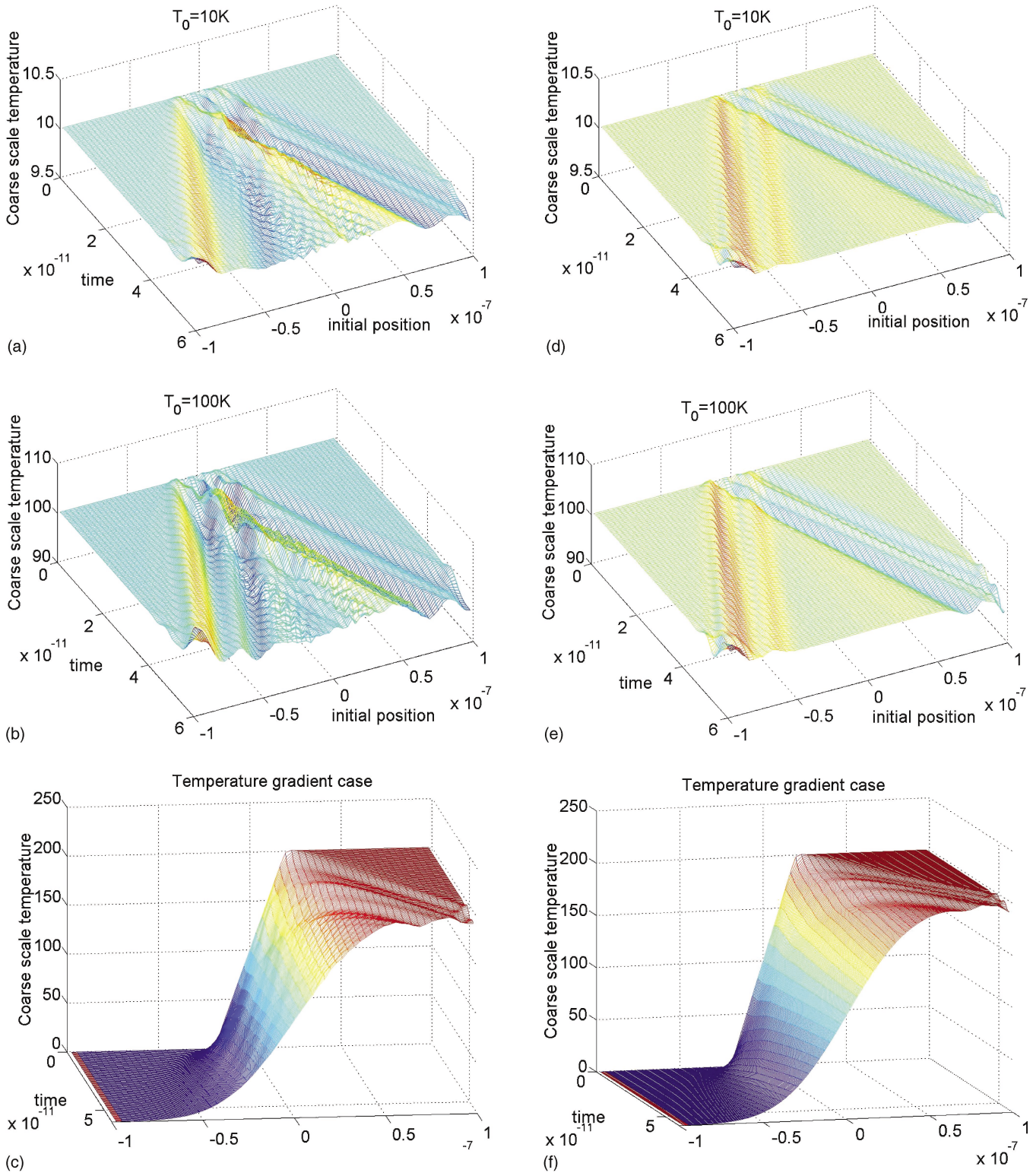

FIG. 6. (Color) Simulations of thermal activation of dislocation. (Coarse scale temperature histories) Multiscale simulations: (a) $T_0=10$ K, (b) $T_0=100$ K, and (c) temperature gradient case. Macroscale simulations: (d) $T_0=10$ K, (e) $T_0=100$ K, and (f) nonuniform initial temperature.

motion toward the region with higher temperature. Moreover, the slope of the temperature distribution reduces with time, which indicates that the steady-state, coarse scale heat diffusion phenomenon is correctly captured and predicted by the proposed nonequilibrium multiscale algorithm. Again, the multiscale simulation results are compared with the macroscale-only simulation results: Figs. 6(d)–6(f). One may find that the coarse scale temperature evolutions are visibly different for two types of simulations, and these differences are solely attributed to the fine scale temperature fluctation. It should be noted that both the heat conductivity coefficient and the specific heat coefficients are evaluated based on the coarse graining or quasicontinuum thermodynamics, and they are kept the same in both the multiscale simulation and

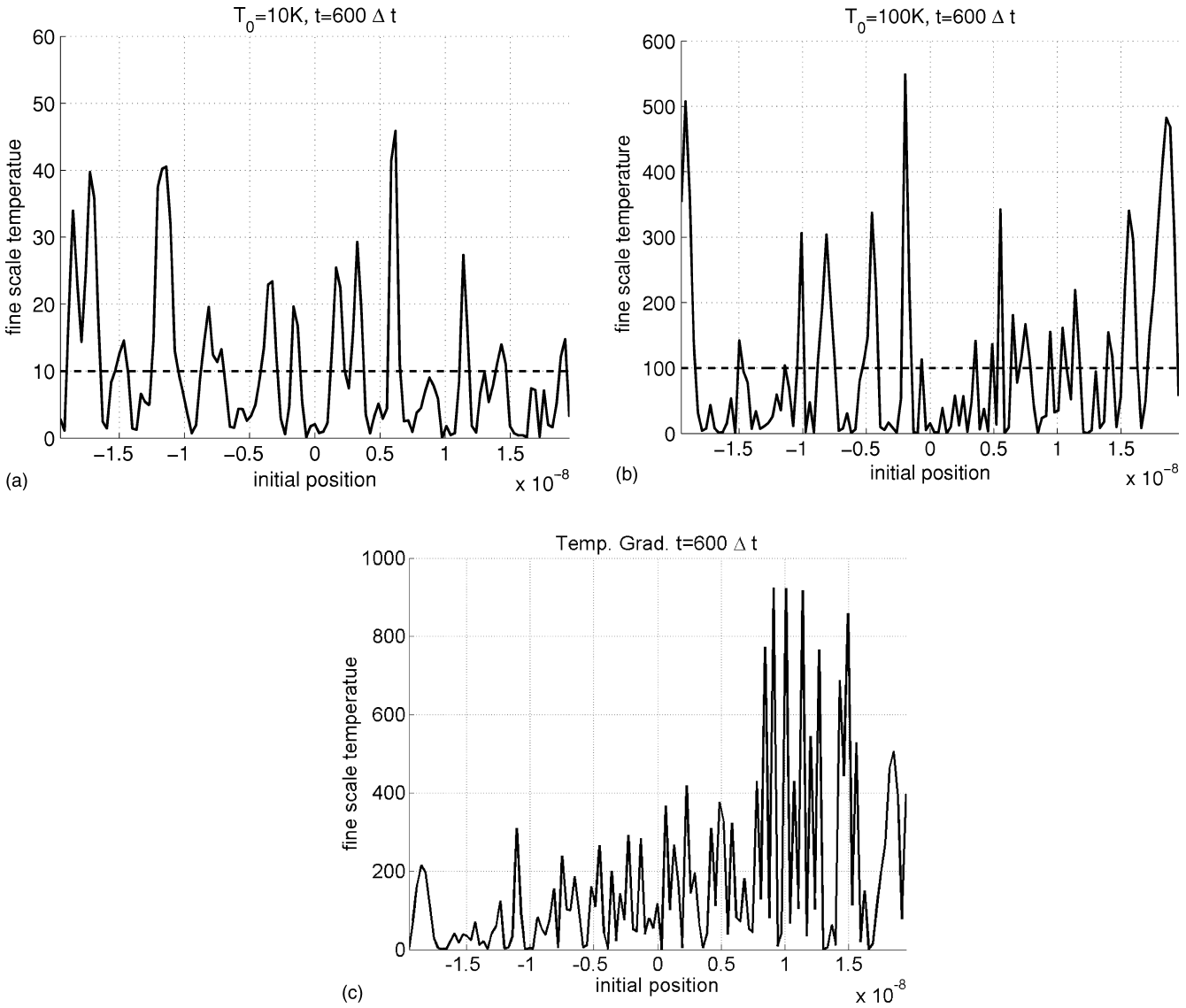

FIG. 7. Instantaneous kinetic temperature (fine scale) profiles at $t=600\Delta t$: (a) $T_0=10$ K, (b) $T_0=100$ K, and (c) temperature gradient case.

the macroscale simulation. Realistically, temperature fluctuation will affect those coefficients as well, which becomes especially significant in small scale. Therefore, those coefficients should be reevaluated after each cycle of coarse scale integration in each finite element. This can be done either based on the transport theory or based on the ratio between heat flux and temperature variance. Only if this procedure is correctly carried out, the proposed multiscale simulation will be a precise nonequilibrium simulation. This part of the work will be reported in the subsequent work.

Figure 7 shows the fine scale temperature distribution at the final time step when the mechanical disturbance has almost passed through fine scale region. We find that the NHC thermostat provides a good temperature control mechanism to maintain correct temperature distributions in the first two cases, i.e., the near constant thermodynamic temperature distribution. For the third case, one can find that qualitatively the kinetic temperature distribution is almost linear over the fine scale region, which is in accordance with the prescribed thermodynamic temperature distribution.

VI. CONCLUSIONS

In this work, a multiscale formulation is proposed to simulate nonequilibrium thermomechanical processes in small scale lattice systems. The proposed nonequilibrium multiscale model not only provides a means to perform concurrent multiscale simulations of relative large system with local atomistic resolution but also reproduces the correct underlying statistical physics. Both aspects have been the challenges in the multiscale computation. The proposed multiscale formulation connects the fine scale statistical mechanics to the coarse scale deterministic responses. It has been shown that the proposed multiscale formulation can accurately capture the coarse scale mean field, and it can also provide the fine scale fluctuations in localized regions.

The proposed model also raises many questions for the multiscale simulation from both theoretical aspects and numerical aspects. For example, how should we relate and utilize linear response theory in a multiscale simulation? These questions shall be addressed in future researches.

ACKNOWLEDGMENT

This work is supported by a grant from NSF (Grant No. CMS-0239130), which is greatly appreciated.

[1] W. A. Curtin and R. E. Miller, Modell. Simul. Mater. Sci. Eng. **11**, R33 (2003).
[2] W. K. Liu, E. G. Karpov, S. Zhang, and H. S. Park, Comput. Methods Appl. Mech. Eng. **193**, 1529 (2004).
[3] L. Dupuy, E. B. Tadmor, R. E. Miller, and R. Phillips, Phys. Rev. Lett. **95**, 060202 (2005).
[4] X. Li and W. E, J. Mech. Phys. Solids **53**, 1650 (2005).
[5] R. E. Rudd and J. Q. Broughton, Phys. Rev. B **72**, 144104 (2005).
[6] B. Shiari, L. E. Miller, and W. A. Curtin, ASME J. Eng. Mater. Technol. **127**, 358 (2005).
[7] M. Zhou, Int. J. Multiscale Comp. Eng. **3**, 177 (2005).
[8] W. G. Hoover, Annu. Rev. Phys. Chem. **34**, 103 (1983).
[9] D. J. Evans and G. P. Morriss, *Statistical Mechanics of Nonequilibrium Liquids* (Academic, San Diego, 1990).
[10] W. G. Hoover and C. G. Hoover, Condens. Matter Phys. **8**, 247 (2005).
[11] D. J. Evans, Phys. Lett. **91A**, 457 (1982).
[12] F. Zhang, D. J. Isbister, and D. J. Evans, Phys. Rev. E **61**, 3541 (2000).
[13] M. Zhang, E. Lussetti, L. E. S. de Souza, and F. Müller-Plathe, J. Phys. Chem. B **109**, 15060 (2005).
[14] W. G. Hoover, D. J. Evans, R. B. Hickman, A. J. C. Ladd, W. T. Ashrst, and B. Moran, Phys. Rev. A **22**, 1690 (1980).
[15] D. J. Evans and G. P. Morriss, Phys. Rev. A **30**, 1528 (1984).
[16] B. J. Edwards, C. Baig, and D. J. Keffer, J. Chem. Phys. **123**, 114106 (2005).
[17] W. G. Hoover, in *Systems Far from Equilibrium*, edited by L. Garrido (Springer-Verlag, Berlin, 1980), pp. 373–380.
[18] R. E. Rudd and J. Q. Broughton, Phys. Rev. B **58**, R5893 (1998).
[19] I. Goldhirsch and C. Goldenberg, Eur. Phys. J. E **9**, 245 (2002).
[20] R. E. Miller and E. B. Tadmor, J. Comput.-Aided Mater. Des. **9**, 203 (2003).
[21] E. Tadmor, M. Ortiz, and R. Phillips, Philos. Mag. A **73**, 1529 (1996).
[22] W. Cai, M. Koning, V. Bulatov, and S. Yip, Phys. Rev. Lett. **85**, 3213 (2000).
[23] H. S. Park, E. G. Karpov, and W. K. Liu, Int. J. Numer. Methods Eng. **64**, 237 (2005).
[24] G. J. Wagner, E. G. Karpov, and W. K. Liu, Comput. Methods Appl. Mech. Eng. **193**, 1579 (2004).
[25] W. E and Z. Huang, Phys. Rev. Lett. **87**, 135501 (2001).
[26] X. Li and W. E, Comput. Phys. Commun. **1**, 136 (2006).
[27] A. To and S. Li, Phys. Rev. B **72**, 035414 (2005).
[28] S. Li, X. Liu, A. Agrawal, and A. To, Phys. Rev. B **74**, 045418 (2006).
[29] J. H. Weiner, *Statistical Mechanics of Elasticity* (Wiley, New York, 1983).
[30] D. J. Diestler, Phys. Rev. B **66**, 184104 (2002).
[31] Z.-B. Wu, D. J. Diestler, R. Feng, and X. C. Zeng, J. Chem. Phys. **119**, 8013 (2003).
[32] H. Jiang, Y. Huang, and K. C. Hwang, ASME J. Eng. Mater. Technol. **127**, 408 (2005).
[33] M. Born and K. Huang, *Dynamical Theory of Crystal Lattices* (Clarendon, Oxford, 1954).
[34] W. Nowacki, *Thermoelasticity*, 2nd ed. (Pergamon, New York, 1986).
[35] C. Kittel, *Introduction to Solid State Physics*, 8th ed. (Wiley, Hoboken, NJ, 2005).
[36] T. J. R. Hughes, *The Finite Element Method: Linear Static and Dynamic Finite Element Analysis* (Prentice-Hall, Englewood Cliffs, NJ, 1987).
[37] O. C. Zienkiewicz and R. L. Taylor, *The Finite Element Method* Solid Mechanics Vol. 1, 5th ed. (Butterworth-Heinemann, Oxford, 2000).
[38] W. G. Hoover, A. J. C. Ladd, and B. Moran, Phys. Rev. Lett. **48**, 1818 (1982).
[39] D. J. Evans, J. Chem. Phys. **78**, 3297 (1983).
[40] S. Nosé, Mol. Phys. **52**, 255 (1984).
[41] W. G. Hoover, Phys. Rev. A **31**, 1695 (1985).
[42] G. J. Martyna, M. L. Klein, and M. E. Tuckerman, J. Chem. Phys. **97**, 2635 (1992).
[43] B. L. Holian, A. F. Voter, and R. Ravelo, Phys. Rev. E **52**, 2338 (1995).
[44] A. C. Brańka, Phys. Rev. E **61**, 4769 (2000).
[45] D. J. Evans, D. J. Searles, W. G. Hoover, C. G. Hoover, B. L. Holian, H. A. Posh. and G. P. Morris, J. Chem. Phys. **108**, 4351 (1998).
[46] M. E. Tuckerman, C. J. Mundy, S. Balasubramanian, and M. L. Klein, J. Chem. Phys. **108**, 4353 (1998).
[47] D. Frenkel and B. Smit, *Understanding Molecular Simulation: From Algorithm to Applications*, 2nd ed. (Academic, New York, 2002).
[48] W. G. Hoover, *Computational Statistical Mechanics* (Elsevier, New York, 1990).
[49] G. J. Wagner and W. K. Liu, J. Comput. Phys. **190**, 249 (2003).
[50] W. K. Liu, E. G. Kapov, S. Zhang, and H. S. Park, Comput. Methods Appl. Mech. Eng. **195**, 1407 (2006).
[51] S. Li, X. Liu, and N. Sheng, Phys. Rev. Lett. (submitted).
[52] S. Jang and G. A. Voth, J. Chem. Phys. **107**, 9514 (1997).
[53] M. E. Tuckerman and G. J. Martyna, J. Chem. Phys. **110**, 3623 (1999).
[54] S. Jang and G. A. Voth, J. Chem. Phys. **110**, 3626 (1999).
[55] G. J. Martyna, M. E. Tuckerman, D. J. Tobias, and M. L. Klein, Mol. Phys. **87**, 1117 (1996).
[56] I. M. Torrens, *Interatomic Potentials* (Academic, New York, 1972).
[57] X. P. Xiao and T. Belytschko, Comput. Methods Appl. Mech. Eng. **193**, 1645 (2004).